Full Length Research Paper

Lineament mapping using multispectral remote sensing satellite data

Maged Marghany* and Mazlan Hashim

Institute of Geospatial Science and Technology (INSTEG), Universiti Teknologi Malaysia 81310 UTM, Skudai, JohoreBahru, Malaysia.

The main objective of this work is to design an automatic image processing tool for lineament mapping from LANDSAT-TM satellite data. In doing so, three procedures are involved: (i) image enhancement using histogram equalization technique; (ii) automatic lineament detection using Canny algorithm; and (iii) three-dimensional (3D) lineament visualization using SRTM data. The study shows that Canny algorithm provides perfect information about lineaments with 3D image visualization which is reconstructed using SRTM. In conclusion, 3D image visualization can provide excellent information about lineament and geological features from remote sensing satellite data.

Key words: LANDSAT TM satellite data, lineament, Canny algorithm, three-dimensional (3D) reconstruction.

INTRODUCTION

Accurate geological features mapping is a critical task for oil exploration, groundwater storage and understanding the mechanisms of environmental disasters, for instance, earthquake, flood and landslides. The major task of geologists is documentation of temporal and spatial variations in the distribution and abundance of geological features over wide scale. In this context, the major challenge is that most of the conventional geological surveying techniques are not able to cover a wide region, such as, desert in the earth's surface. Quite clearly, to understand the mechanisms generations of geological features and their relationship with environmental disasters such as earthquake, landslide and flood, geological researchers must be able to conduct simultaneous measurements over broad areas of the surface or subsurface of the earth (Maged et al., 2009). This requires the collection of asset of reliable synoptic data that specify variations of critical geological environmental parameters over a wide region for discrete moments. In fact, geological features such as lineament and faults are key parameters that described the earth's generation or disaster mechanisms and are a significant indicator for oil explorations and groundwater storages

(Semere and Ghebreab, 2006). Fortunately, the application of remote-sensing technology from space is providing geologists with means of acquiring these synoptic data sets. Consequently, optical remote sensing techniques over three decades have shown a great promise for mapping geological feature variations over a wide scale (Mostafa and Bishta, 2005; Semere and Ghebreab, 2006; Maged et al., 2009). In referring to Katsuaki et al. (1995) and Walsh (2000), lineament information extractions in satellite images can be divided broadly into three categories: (i) lineament enhancement and extraction for the characterization of the geologic structure; (ii) image classification to perform the geologic mapping or locate spectrally, anomalous zones attributable to mineralization (Mostafa et al., 1995; Süzen and Toprak, 1998) and (iii) superposition of satellite images and multiple data such as geological, geochemical and geophysical data in a geographical information system (Novak and Soulakellis, 2000; Semere and Ghebreab, 2006). Furthermore, remote sensing data assimilation in real time could be a bulk tool for geological features extraction and mapping. In this context, several investigations are currently underway on the assimilation of both passive and active remotely sensed data into automatic detection of significant geological features, that is, lineament, curvilinear and fault.

---

*Corresponding author. E-mail: magedupm@hotmail.com.
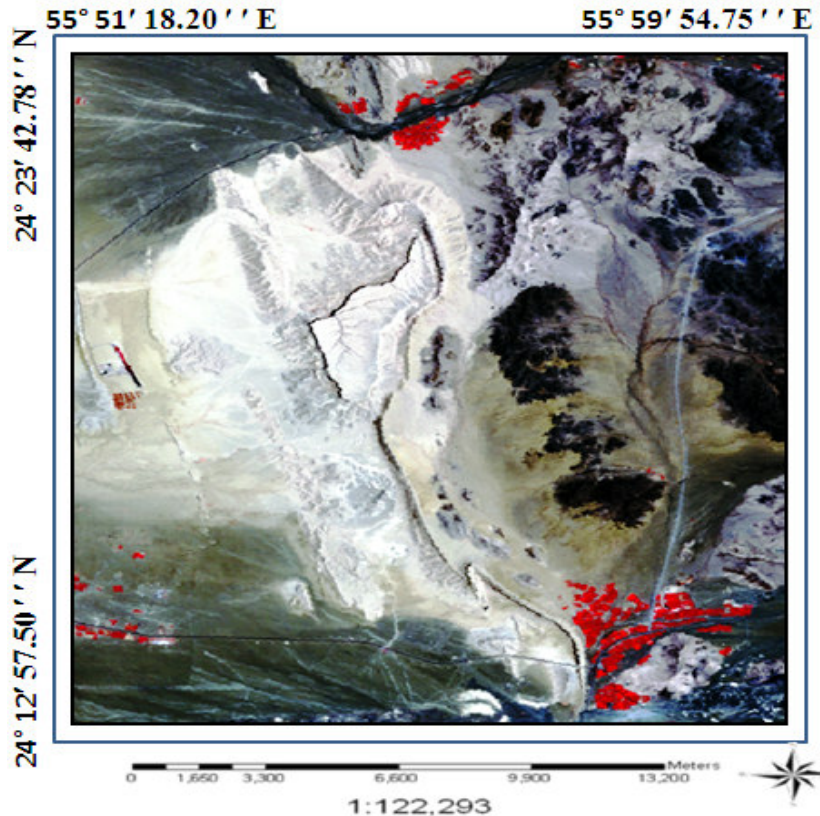
Figure 1. Location of the study area.

Image processing tools that have been used for lineament feature detections are: (i) image enhancement techniques (Mah et al., 1995; Chang et al., 1998; Walsh, 2000; Maged et al., 2009) and (ii) edge detection and segmentation (Wang et al., 1990; Vassilas et al., 2002; Mostafa and Bishta, 2005). In practice, researchers have preferred to use the spatial domain filtering techniques in order to get rid of the artificial lineaments and to verify disjoint lineament pixels in satellite data (Süzen and Toprak, 1998). Further, Leech et al. (2003) implemented the band-rationing, linear and Gaussian nonlinear stretching enhancement techniques to determine lineament populations. Won-In and Charusiri (2003) found that 'high pass filter' enhancement technique provides accurate geological map. In fact, the 'high pass filter' selectively enhances the small scale features of an image (high frequency spatial components), while maintaining the larger-scale features (low frequency components) that constitute most of the information in the image.

Majumdar and Bhattacharya (1998) and Vassilas et al. (2002), respectively have used Haar and Hough transforms as edge detection algorithms for lineament detection in Landsat-TM satellite data. Majumdar and Bhattacharya (1998) reported that Haar transform is proper in the extraction of subtle features with finer details from satellite data. Vassilas et al. (2002),

however, reported that Hough transform is appropriate for fault feature mapping. Consequently, Laplacian, Sobel and Canny are the major algorithms for lineament feature detections in remotely sensed data (Mostafa and Bishta, 2005; Semere and Ghebreab, 2006; Maged et al., 2009). This study aims to introduce a comprehensive tool for 3D lineament detection and visualization in satellite remote sensing data. This tool is the function of integration between Canny edge detection algorithm and digital elevation model which is produced using SRTM data.

RESEARCH METHODS

Study area

The study area is located in Sharjah Emirates about 70 Km from Sharjah city. It is considered in the alluvium plain for the central area of UAE and covers an area of 1800 Km^2 (60 x 30 km) within boundaries of latitudes 24º 12'N to 24º.23'N and longitudes 55º.51'E to 55º 59' E (Figure 1). The northern part of UAE is formed from the Oman mountains and the marginal hills extends from the base of the mountains and (alluvium plain) to the south western sand dunes. Land geomorphology is composed of structural form, fluvial and Aeolian forms (sand dunes). According to Maged et al., (2009) structural form is a broad part of the Oman mountains and JabalFayah, which are folded structures, due to collusion of oceanic crust and Arabian plate (continental plate). Furthermore, the mountain is raised higher than 400 m above sea level and exhibit parallel ridges and high–tilted beds. Many valleys are cut down the
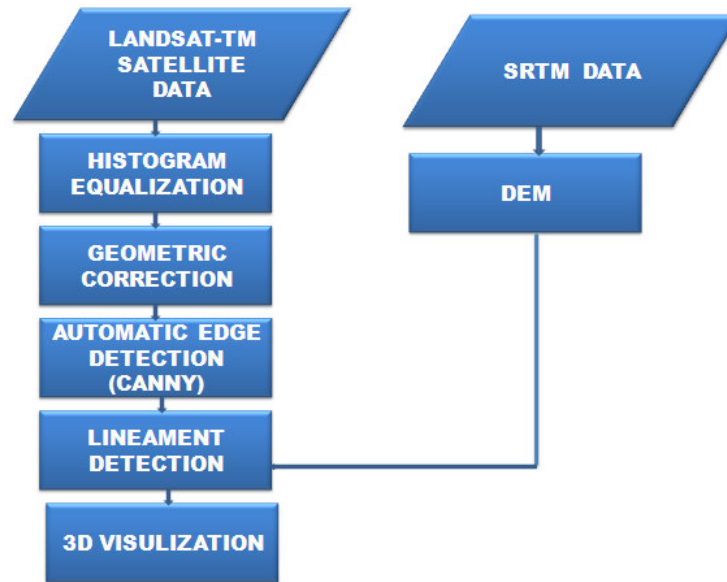
Figure 2. Flow chart of lineament mapping from LANDSAT-TM satellite data.

mountains, forming narrow clefts and there are also intermittent basins caused by differential erosion. In addition, the valley bases are formed from small caves.

Data set

The satellite data used in this study are acquired from LANDSAT-TM, which covered an area located between latitudes 24º 12′N to 24º.23'N and longitudes 55º.51'E to 55º 59' E (Figure 1). Bands 1,2,3,5 and 7 are selected to achieve the objective of this study. According to Maged et al. (2009), these bands can provide accurate geological information. Finally, the Digital Elevation Model (DEM) is acquired from SRTM data.

Lineament extraction procedures

Here, the procedures that have been used to extract lineaments pattern from LANDSAT TM satellite images are described. Following Maged et al. (2009), image enhancement contrast, stretching and linear enhancement are applied to acquire an excellent visualization. In addition, automatic detection algorithm of Canny is then used to acquire lineament mapping (Figure 2).

Histogram equalization

Following Maged et al. (2009), histogram equalization is applied to LANDSAT TM image to obtain high quality image visualization. An image histogram is an analytic tool used to measure the amplitude distribution of pixels within an image. For example, a histogram can be used to provide a count of the number of pixels at amplitude 0, the number at amplitude 1, and so on. By analyzing the distribution of pixel amplitudes, some information about the visual appearance of an image can be gained. A high-contrast image contains a wide distribution of pixel counts covering the entire amplitude range, while a low contrast image has most of the pixel amplitudes congregated in a relatively narrow range (Süzen et al., 1998; Gonzalez and Woods, 1992).

Canny algorithm procedures

According to Canny (1986), the Canny edge detector uses a filter based on the first derivative of a Gaussian, because it is susceptible to noise that is present on the raw unprocessed image data. So to begin with, the raw image is convolved with a Gaussian filter. The result is a slightly blurred version of the original which is not affected by a single noisy pixel to any significant degree. According to Deriche (1987), the edge detection operator (Roberts, Prewitt and Sobel for example) returns a value for the first derivative in the horizontal (G_y) and vertical direction (G_x). From this, the edge gradient and direction (Ө) can be determined:

$$|G| = \sqrt{G_x{}^2 + G_y{}^2} \tag{1}$$

In fact, Equation 1 is used to estimate the gradient magnitude (edge strength) at each point that can be seen to find the edge strength by taking the gradient of the image. Typically, an approximate magnitude is computed using

$$|G| = |G_x| + |G_y| \tag{2}$$

Equation 2 is faster to be computed.

$$\theta = \arctan\left(\frac{G_y}{G_x}\right) \tag{3}$$

The direction of the edge, θ, is computed using the gradient in the G_x and G_y directions. However, an error will be generated when sum X is equal to zero. So in the code, there has to be a restriction set whenever this takes place. Whenever the gradient (G) in the x direction is equal to zero, the edge direction has to be equal to 90 or 0°, depending on what the value of the gradient in the y-direction is equal to. If G_y has a value of zero, the edge direction will equal 0°; otherwise, the edge direction will equal 90° (Deriche 1987).

According to Gonzalez and Woods (1992), three criteria are used to improve edge detection. The first and most obvious is the low error rate. It is important that the edges occurring in images should not be missed and that there should be no responses to non-edges. The second criterion is that the edge points should be well localized. In other words, the distance between the edge pixels as found by the detector and the actual edge is to be at a minimum. A third criterion is to have only one response to a single edge. This was implemented because the first 2 were not substantial enough to completely eliminate the possibility of multiple responses to an edge (Canny, 1986).

RESULTS AND DISCUSSION

Figure 3 shows that the 'digital elevation model' is derived from SRTM data. Clearly, DEM varies between 319 to 929 m and the maximum elevation value of 929 m is found in the northeast direction of UAE. This result confirms the study of Maged et al. (2009).

Figure 4 shows the supervised classification map of LANDSAT TM satellite data. It is clear that the vegetation covers are located in the highest elevation as compared with Figure 3, while highlands are located in the lowest elevation with a DEM value of 660 m. The supervised classification shows that a great fault moves through a highland area.

Figure 5 shows the output result mapping of lineaments using composite of bands 3, 4, 5 and 7 in LANDSAT TM satellite data. The appearance of lineaments in LANDSAT TM satellite image is clearly distinguished. In addition, the area adjacent to the mountains from Manamh (northward) and Flili village (southward), has high density of lineaments due to the westward compressive force between the oceanic crust and Arabian plate, such as fractures and faults and drainage pattern that runs in the buried fault plains (filled weathered materials coming from Oman mountains) (Figure 5). The lineaments are associated with fractures and faults which are located in the northern part of Figure 5. In fact, Canny algorithm is first used to smooth the image and eliminate the noise. It then finds the image gradient to highlight regions with high spatial derivatives. The algorithm then tracks along these regions and suppresses any pixel that is not at the maximum (non-maximum suppression). The gradient array is further reduced by hysteresis. According to Deriche (1987), hysteresis is used to track along the remaining pixels that have not been suppressed. Hysteresis uses two thresholds and if the magnitude is below the first threshold, it is set to zero (made a non-edge). Further, if the magnitude is above the high threshold, it is made to an edge and if the magnitude is between the 2 thresholds, then it is set to zero unless there is a path from this pixel to a pixel with a gradient above threshold. In order to implement the Canny edge detector algorithm, a series of steps must be followed. The first step is to filter out any noise in the original image before trying to locate and detect any edges. In fact, the Gaussian filter

can be computed using a simple mask and is used exclusively in the Canny algorithm. Once a suitable mask has been calculated, the Gaussian smoothing can be performed using standard convolution methods.

According to Maged et al. (2009), LANDSAT TM data can be used to map geological features such as lineaments and faults. This could contribute to the composite of bands 3, 4, 5 and 7 in LANDSAT TM satellite data that are appropriate for mapping of geologic structures (Katsuaki and Ohmi, 1995; Novak and Soulakellis, 2000; Maged et al., 2009). Consequently, the ground resolution cell size of LANDSAT TM data is about 30 m.

Figure 6 shows the lineament distribution with 3D map reconstruction using SRTM and LANDSAT TM bands 3, 4, 5 and 7. It is clear that the 3D visualization discriminates between different geological features. However, the faults, lineament and infrastructures can be noticed clearly (Figure 6b). Moreover, this study agrees with Maged et al. (2009). It can be confirmed that the lineament are associated with faults and it also obvious that heavy capacity of lineament occurrences is within the Oman mountain. This type of lineament can be named as mountain lineament.

According to Maged et al. (2009) the mountain is raised higher than 400 m above sea level and exhibit parallel ridges and high-tilted beds. Many valleys are cut down the mountains, forming narrow clefts and small caves. The fluvial forms are consisted of streams channels which flowed from Oman mountains and spread out into several braided channels at the base of the mountains from the Bahada and Playa plains (Figure 7). Stream channels have been diverted to the southwest and they deposited silt in the tongue -shaped which lies between the dunes.

Further, Aeolian forms are extended westwards from the Bahada plain, where liner dunes run towards the southwest direction in parallel branching pattern (Figure 3) with relative heights of 50 m. Nevertheless, the heights are decreased towards the southeast due to a decrease in sand supply and erosion caused by water occasionally flowing from the Oman Mountains. Moreover, some of the linear dunes are quite complex due to the development of rows of star dunes along the top of their axes. Additionally, inter dunes areas are covered by fluvial material which are laid down in the playas formed at the margins of the Bahadas plain near the coastline. The dunes changes their forms to low flats of marine origin and their components are also dominated by bioclastics and quartz sands (Maged et al., 2009).

Conclusions

This study has demonstrated a method to map lineament distributions in United Arab Emirates (UAE) using LANDSAT-TM satellite data. In doing so, 3D image
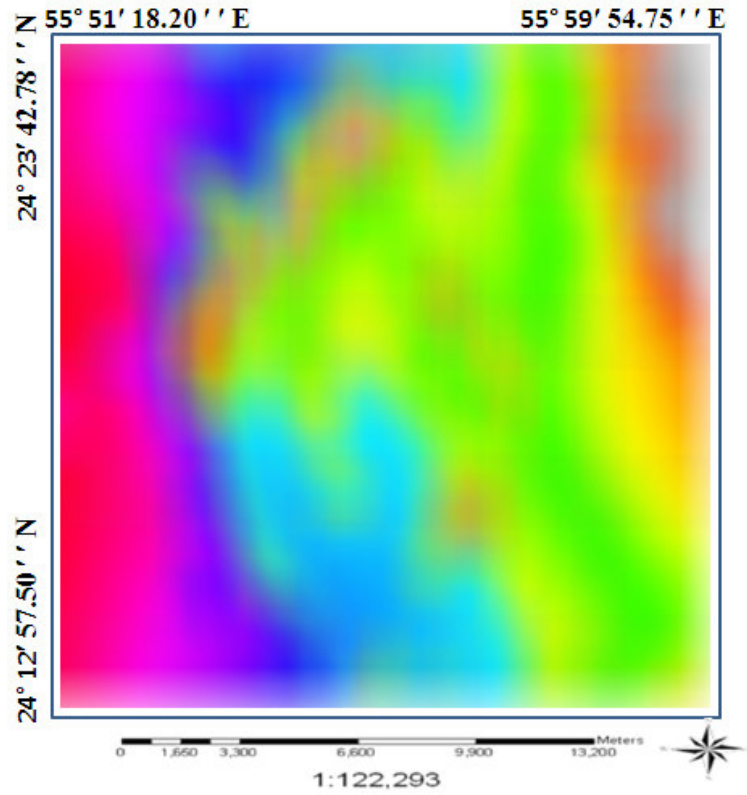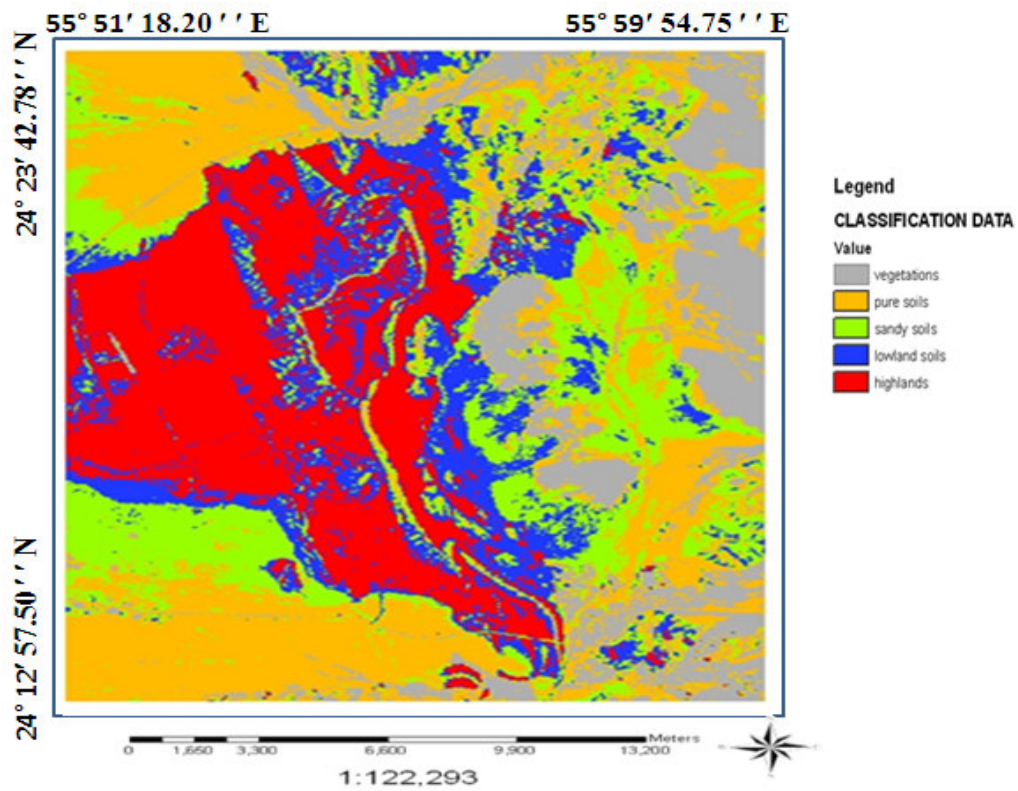
Figure 3. DEM for the study area.
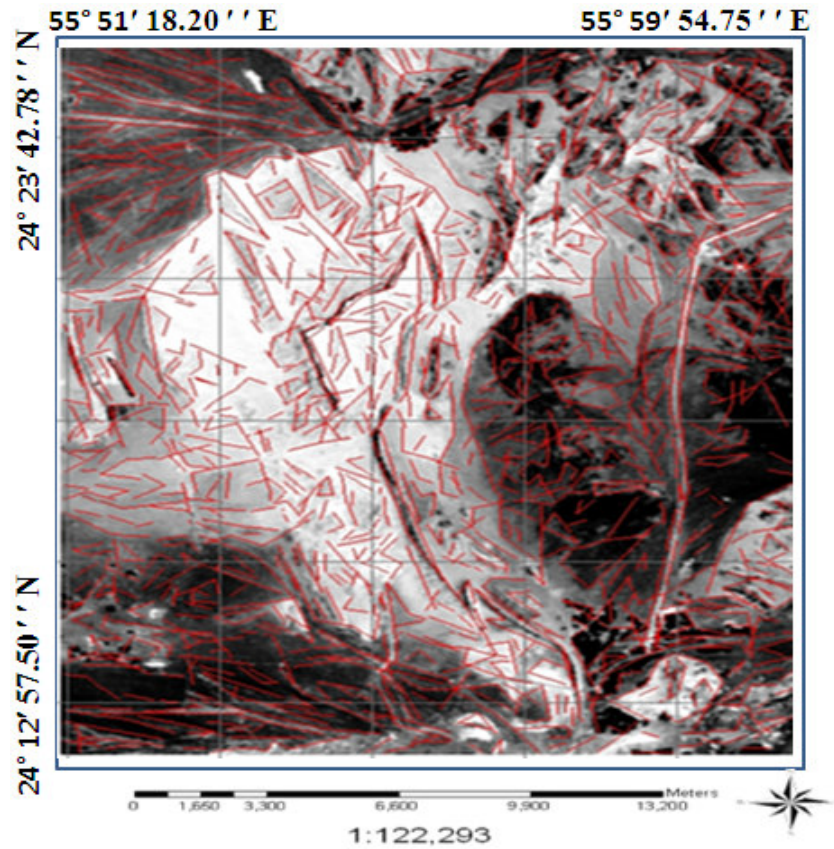

Figure 4. Supervised map results.

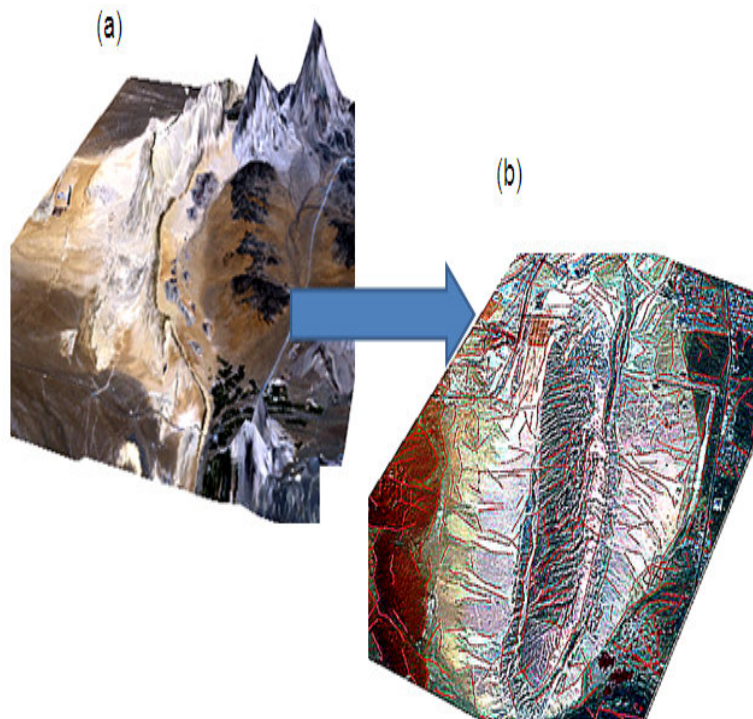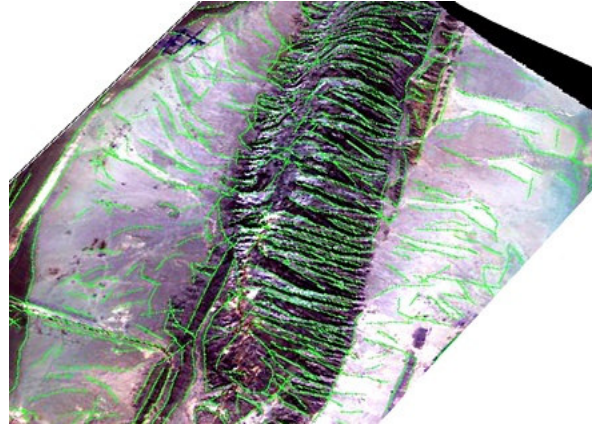**Figure 5.** Lineament mapping using Canny algorithm.

Figure 6. (a) 3D image reconstruction using SRTM data and (b) lineament distribution over 3D image.

Figure 7. 3D image and lineament distribution from Canny algorithm.

reconstruction is produced using SRTM data. Then Canny algorithm is implemented for lineament automatic detection from LANDSAT TM bands of 3, 4, 5 and 7. The results show that the maximum DEM value of 929 m is found in the northeast direction of UAE. The vegetation covers are the dominant feature in the highest DEM, while highlands are located in the lowest elevation of 660 m. In addition, Canny algorithm has detected automatically, lineament and fracture features. Therefore, 3D visualization is discriminated between lineament and fault features. The results show that the highest spatial distribution of lineaments appeared in Oman mountain, which are named lineament mountain. In conclusion, the integration between 'digital elevation model' (DEM) and Canny algorithm can be used as a geomatic tool for lineament automatic detection in 3D visualization.

REFERENCES

Canny JA (1986). Computational Approach To Edge Detection. IEEE Transactions on Pattern Analysis and Machine Intelligence. PAMI, 8(6): 679-698.

Chang Y, Song G, Hsu S (1998). Automatic Extraction of Ridge and Valley Axes Using the Profile Recognition and Polygon-Breaking Algorithm. Comput. Geosci., 24(1): 83-93.

Deriche R (1987). Using Canny's criteria to derive a recursively implemented optimal edge detector. Int. J. Comput. Vision. 1(2): 167-187.

Gonzalez R, Woods R (1992). Digital Image Processing, 3rd edition (March 1992), Addison-Wesley Publishing Company, pp. 200-229.

Katsuaki K, Shuichi N, Ohmi M (1995). Lineament analysis of satellite images using a segment tracing algorithm (STA). Comput. Geosci., 21(9): 1091-I 104.

Leech DP, Treloar PJ, Lucas NS, Grocott J (2003). Landsat TM analysis of fracture patterns: a case study from the Coastal Cordillera of northern Chile. Int. J. Remote Sensing, 24(19): 3709-3726.

Maged M, Mansor S, Hashim M (2009). Geologic mapping of United Arab Emirates using multispectral remotely sensed data. Amer. J. Eng. Appl. Sci.. 2: 476-480.

Mah A, Taylor GR, Lennox P, Balia L (1995). Lineament Analysis of Landsat Thematic Mapper Images, Northern Territory, Australia. Photogramm. Eng. Remote Sensing, 61(6): 761-773.

Majumdar TJ, Bhattacharya BB (1988). Application of the Haar transform For extraction of linear and anomalous over part of Cambay Basin, India. Int. J. Remote Sensing, 9(12): 1937-1942.

Mostafa ME, Bishta AZ (2005). Significant of lineament pattern in rock unit classification and designation: A pilot study on the gharib-dara area. Northen eastern Desert, Egypt. Int. J. Remote Sensing, 26(7): 1463 - 1475.

Mostafa ME, Qari MYHT (1995). An exact technique of counting lineaments. Eng. Geol., 39(1-2): 5-15.

Novak ID, Soulakellis N (2000). Identifying geomorphic features using Landsat-5/TM data processing techniques on lesvos, Greece. Geomorphol., 34: 101-109.

Semere S, Ghebreab W (2006). Lineament characterization and their tectonic significance using Landsat TM data and field studies in the central highlands of Eritrea. J. Afr. Earth Sci., 46(4): 371-378.

Süzen ML, Toprak V (1998). Filtering of satellite images in geological lineament analyses: An application to a fault zone in central Turkey. Int. J. Remote Sensing, 19(6): 1101-1114.

Vassilas N, Perantonis S, Charou E, Tsenoglou T, Stefouli M, Varoufakis S (2002). Delineation of Lineaments from Satellite Data Based on Efficient Neural Network and Pattern Recognition Techniques. 2nd Hellenic Conf. on AI, SETN-2002, 11-12 April 2002, Thessaloniki, Greece, Proceedings, Companion Vol. 355-366.

Walsh GJ, Clark Jr SF (2000). Contrasting methods of fracture trend characterization in crystalline metamorphic and igneous rocks of the Windham quadrangle, New Hampshire. Northeast. Northeastern Geol. Environ. Sci., 22(2): 109-120.

Won-In K, Charusiri P (2003). Enhancement of thematic mapper satellite images for geological mapping of the Cho Dien area, Northern Vietnam. Int. J. Appl. Earth Observ. Geoinf., 15: 1-11.